

Neutron-Proton Scattering in the Context of the $d^*(2380)$ Resonance

P. Adlarson,¹ W. Augustyniak,² W. Bardan,³ M. Bashkanov,^{4,5} F.S. Bergmann,⁶ M. Berłowski,⁷ H. Bhatt,⁸ M. Büscher,^{9,10} H. Calén,¹ I. Ciepał,³ H. Clement,^{4,5} D. Coderre,^{11,12,13,*} E. Czerwiński,³ K. Demmich,⁶ E. Doroshkevich,^{4,5} R. Engels,^{11,12} A. Erven,^{14,12} W. Erven,^{14,12} W. Eyrich,¹⁵ P. Fedorets,^{11,12,16} K. Föhl,¹⁷ K. Fransson,¹ F. Goldenbaum,^{11,12} P. Goslawski,⁶ A. Goswami,^{11,12,18} K. Grigoryev,^{12,19,20} C.-O. Gullström,¹ F. Hauenstein,¹⁵ L. Heijkinskjöld,¹ V. Hejny,^{11,12} M. Hodana,³ B. Höistad,¹ N. Hüsen,⁶ A. Jany,³ B.R. Jany,³ L. Jarczyk,³ T. Johansson,¹ B. Kamys,³ G. Kemmerling,^{14,12} F.A. Khan,^{11,12} A. Khoukaz,⁶ D.A. Kirillov,²¹ S. Kistryn,³ H. Kleines,^{14,12} B. Kłos,²² M. Krapp,¹⁵ W. Krzemień,³ P. Kulesa,²³ A. Kupść,^{1,7} K. Lalwani,^{8,†} D. Lersch,^{11,12} B. Lorentz,^{11,12} A. Magiera,³ R. Maier,^{11,12} P. Marciniowski,¹ B. Mariański,² M. Mikirtychiants,^{11,12,13,20} H.-P. Morsch,² P. Moskal,³ H. Ohm,^{11,12} I. Ozerianska,³ E. Perez del Rio,^{4,5} N.M. Piskunov,²¹ P. Podkopał,³ D. Prasuhn,^{11,12} A. Pricking,^{4,5} D. Pszczel,^{1,7} K. Pysz,²³ A. Pyszniak,^{1,3} C.F. Redmer,^{1,‡} J. Ritman,^{11,12,13} A. Roy,¹⁸ Z. Rudy,³ S. Sawant,^{8,11,12} S. Schadmand,^{11,12} T. Sefzick,^{11,12} V. Serdyuk,^{11,12} V. Serdyuk,^{11,12,24} R. Siudak,²³ T. Skorodko,^{4,5,25} M. Skurzok,³ J. Smyrski,³ V. Sopov,¹⁶ R. Stassen,^{11,12} J. Stepaniak,⁷ E. Stephan,²² G. Sterzenbach,^{11,12} H. Stockhorst,^{11,12} H. Ströher,^{11,12} A. Szczurek,²³ A. Täschner,⁶ A. Trzeciński,² R. Varma,⁸ G.J. Wagner,^{4,5} M. Wolke,¹ A. Wrońska,³ P. Wüstner,^{14,12} P. Wurm,^{11,12} A. Yamamoto,²⁶ L. Yurev,^{24,§} J. Zabierowski,²⁷ M.J. Zieliński,³ A. Zink,¹⁵ J. Złomańczuk,¹ P. Żuprański,² and M. Żurek^{11,12}
(WASA-at-COSY Collaboration)

R. L. Workman,²⁸ W. J. Briscoe,²⁸ and I. I. Strakovsky²⁸
(SAID Data Analysis Center)

¹Division of Nuclear Physics, Department of Physics and Astronomy, Uppsala University, Box 516, 75120 Uppsala, Sweden

²Department of Nuclear Physics, National Centre for Nuclear Research, ul. Hoza 69, 00-681, Warsaw, Poland

³Institute of Physics, Jagiellonian University, ul. Reymonta 4, 30-059 Kraków, Poland

⁴Physikalisches Institut, Eberhard-Karls-Universität Tübingen, Auf der Morgenstelle 14, 72076 Tübingen, Germany

⁵Kepler Center for Astro and Particle Physics, University of Tübingen, Auf der Morgenstelle 14, 72076 Tübingen, Germany

⁶Institut für Kernphysik, Westfälische Wilhelms-Universität Münster, Wilhelm-Klemm-Str. 9, 48149 Münster, Germany

⁷High Energy Physics Department, National Centre for Nuclear Research, ul. Hoza 69, 00-681, Warsaw, Poland

⁸Department of Physics, Indian Institute of Technology Bombay, Powai, Mumbai-400076, Maharashtra, India

⁹Peter Grünberg Institut, Forschungszentrum Jülich, 52425 Jülich, Germany

¹⁰Institut für Laser- und Plasmaphysik, Heinrich-Heine Universität Düsseldorf, 40225 Düsseldorf, Germany

¹¹Institut für Kernphysik, Forschungszentrum Jülich, 52425 Jülich, Germany

¹²Jülich Center for Hadron Physics, Forschungszentrum Jülich, 52425 Jülich, Germany

¹³Institut für Experimentalphysik I, Ruhr-Universität Bochum, Universitätsstr. 150, 44780 Bochum, Germany

¹⁴Zentralinstitut für Engineering, Elektronik und Analytik, Forschungszentrum Jülich, 52425 Jülich, Germany

¹⁵Physikalisches Institut, Friedrich-Alexander-Universität

Erlangen-Nürnberg, Erwin-Rommel-Str. 1, 91058 Erlangen, Germany

¹⁶Institute for Theoretical and Experimental Physics, State Scientific Center of the Russian Federation, Bolshaya Cheremushkinskaya 25, 117218 Moscow, Russia

¹⁷II. Physikalisches Institut, Justus-Liebig-Universität Gießen, Heinrich-Buff-Ring 16, 35392 Giessen, Germany

¹⁸Department of Physics, Indian Institute of Technology Indore, Khandwa Road, Indore-452017, Madhya Pradesh, India

¹⁹III. Physikalisches Institut B, Physikzentrum, RWTH Aachen, 52056 Aachen, Germany

²⁰High Energy Physics Division, Petersburg Nuclear Physics Institute,

Orlova Roshka 2, Gatchina, Leningrad district 188300, Russia

²¹Veksler and Baldin Laboratory of High Energy Physics, Joint

Institute for Nuclear Physics, Joliot-Curie 6, 141980 Dubna, Russia

²²August Chelkowski Institute of Physics, University of Silesia, Uniwersytecka 4, 40-007, Katowice, Poland

²³The Henryk Niewodniczański Institute of Nuclear Physics, Polish

Academy of Sciences, 152 Radzikowskiego St, 31-342 Kraków, Poland

²⁴Dzhelepov Laboratory of Nuclear Problems, Joint Institute for Nuclear Physics, Joliot-Curie 6, 141980 Dubna, Russia

²⁵Department of Physics, Tomsk State University, 634050 Tomsk, Russia

²⁶High Energy Accelerator Research Organisation KEK, Tsukuba, Ibaraki 305-0801, Japan

²⁷Department of Cosmic Ray Physics, National Centre for Nuclear Research, ul. Uniwersytecka 5, 90-950 Łódź, Poland

²⁸Data Analysis Center at the Institute for Nuclear Studies, Department of

Physics, The George Washington University, Washington, D.C. 20052, U.S.A.

(Dated: November 6, 2018)

New data on quasifree polarized neutron-proton scattering, in the region of the recently observed d^* resonance structure, have been obtained by exclusive and kinematically complete high-statistics measurements with WASA at COSY. This paper details the determination of the beam polarization, checks of the quasifree character of the scattering process, on all obtained A_y angular distributions and on the new partial-wave analysis, which includes the new data producing a resonance pole in the 3D_3 - 3G_3 coupled partial waves at $(2380 \pm 10 - i40 \pm 5)$ MeV – in accordance with the d^* dibaryon resonance hypothesis. The effect of the new partial-wave solution on the description of total and differential cross section data as well as specific combinations of spin-correlation and spin-transfer observables available from COSY-ANKE measurements at $T_d = 2.27$ GeV is discussed.

PACS numbers: 13.75.Cs, 13.85.Dz, 14.20.Pt

Keywords:

INTRODUCTION

Recent measurements of the basic double-pionic fusion to the deuteron, which comprises the reaction channels $pn \rightarrow d\pi^0\pi^0$, $pn \rightarrow d\pi^+\pi^-$ and $pp \rightarrow d\pi^+\pi^0$, reveal a narrow resonance-like structure in the total cross section at a mass $M \approx 2380$ MeV with a width of $\Gamma \approx 70$ MeV [1–3]. From the isospin decomposition of the cross sections in the three fusion channels the isoscalar nature of this structure has been determined [3], whereas the determination of its spin-parity $J^P = 3^+$ has been obtained from the angular distributions in the $d\pi^0\pi^0$ channel, which has a particularly low background from conventional reaction processes [2]. Further support for this resonance structure has been found in the $pn \rightarrow pp\pi^0\pi^-$ reaction [4], where it was denoted by d^* – following its notation associated with the so-called "inevitable" dibaryon [5, 6] having identical quantum numbers.

If the observed resonance-like structure constitutes an s -channel resonance in the neutron-proton system, then it has to be sensed also in the observables of elastic np scattering. In Ref. [7] this resonance effect in np scattering has been estimated and it was shown that a noticeable effect should appear in the analyzing power A_y . This observable is most sensitive to small changes in the partial waves, since it is composed only of interference terms between partial waves.

For the analyzing power, there are data only below and above the resonance region. These data sets, at $T_n = 1.095$ GeV ($\sqrt{s} = 2.36$ GeV) [8, 9] and $T_n = 1.27$ GeV ($\sqrt{s} = 2.43$ GeV) [10, 11], exhibit very similar angular distributions. This gap in the existing measurements of A_y has motivated the present study, the main results of which have been communicated recently already in a Letter [12].

EXPERIMENT

The measurements of polarized $\vec{n}p$ elastic scattering over the energy region of interest have been carried out in the quasifree mode. The experiment was performed with the WASA detector [13, 14] at the COSY storage ring by use of a polarized deuteron beam of energy of

$T_d = 2.27$ GeV, which impinged on the WASA hydrogen pellet target. Utilizing the quasifree scattering process the full energy region of the conjectured resonance was covered. Since we observe here the quasi-free scattering process $\vec{d}p \rightarrow np + p_{spectator}$ in inverse kinematics, we were able to detect the fast spectator proton in the forward detector of WASA.

Since elastic np scattering has a large cross section, it was sufficient to have a trigger, which solely requested one hit in the first layer of the forward range hodoscope. Such a hit could originate from either a charged particle or a neutron. For the case of quasifree np scattering we thus have three event classes, with each of them having the spectator proton hit the forward detector:

- (i) Both scattered proton and scattered neutron are detected in the central detector. This event type covers the region $31^\circ < \Theta_n^{cm} < 129^\circ$ of neutron angles.
- (ii) The scattered proton is detected in the forward detector, whereas the scattered neutron is not measured. This type concerns the region $132^\circ < \Theta_n^{cm} < 178^\circ$.
- (iii) The scattered proton is detected in the central detector with the neutron being unmeasured, since its scattering angle is outside the angular range of the central detector. This event type covers the angular range $30^\circ < \Theta_n^{cm} < 41^\circ$.

Thus nearly the full range of neutron scattering angles could be covered by use of all three event classes.

Since by use of inverse kinematics the spectator proton resides in the deuteron beam particle, the emitted spectator proton is very fast, which facilitates its detection in the forward detector. Thus by reconstructing emission angles and kinetic energy the full four-momentum of the spectator proton can be determined.

The four-momentum of the actively scattered proton has been obtained from its track information in either the forward or the central detector. In the latter case the energy information was not retrieved.

In the case that the actively scattered proton has been detected together with its scattering partner, the neutron

(case (i)), we checked in addition, whether the angular correlation for elastic kinematics is fulfilled.

That way we were able to reconstruct the full event, which includes also the four-momentum of the neutron. In the case that the neutron was not measured, the subsequent kinematic fit had one overconstraint in case (ii) and none in case (iii). In the case that the neutron could be detected by a hit in the calorimeter (composed of 1012 CsI(Na) crystals) of the central detector – associated with no hit in the preceding plastic scintillator barrel, the directional information of the scattered neutron could be retrieved. Therefore, such events, which correspond to case (i), have undergone a kinematic fit with two overconstraints.

Determination of the Beam Polarization

In order not to distort the beam polarization, the magnetic field of the solenoid in the central detector was switched off. The measurements have been carried out with cycles of the beam polarization "up", "down" and unpolarized (originating from the same polarized source), where "up" and "down" refers to a horizontal scattering plane. Runs with the conventional unpolarized source verified that the beam originating from the polarized source indeed was unpolarized when using it in its "unpolarized" mode.

The magnitude of the beam polarization has been determined and monitored by dp elastic scattering, which was measured in parallel by detecting the scattered deuteron in the forward detector as well as the associated scattered proton in the central detector. In case of a transversally polarized deuteron beam the dependence of the count rate $N(\Theta, \Phi)$ on the polar and azimuthal scattering angles Θ and Φ is given by

$$N(\Theta, \Phi) \sim 1 + \frac{3}{2}P_z A_y(\Theta)\cos\Phi + \frac{1}{4}P_{zz} [A_{xx}(\Theta)(1 - \cos 2\Phi) + A_{yy}(\Theta)(1 + \cos 2\Phi)]. \quad (1)$$

Here P_z and P_{zz} denote vector and tensor polarization of the deuteron beam, whereas A_y , A_{xx} and A_{yy} are the respective vector and tensor analyzing powers of the dp scattering process.

With WASA covering the full azimuthal angular range, we may decompose vector and tensor parts by fitting the observed azimuthal angular dependence for specific polar angles by use of eq. (1). The absolute values for the vector and tensor components of the deuteron beam have been obtained by fitting our results for the vector A_y (Fig. 1, top) and tensor analyzing power A_{yy} (Fig. 1, bottom) in absolute height to those obtained previously at ANL [15] for $T_d = 2.0$ GeV. Though this energy is somewhat below the one used here, the analyzing powers in pd scattering have been observed [15, 16] to be only

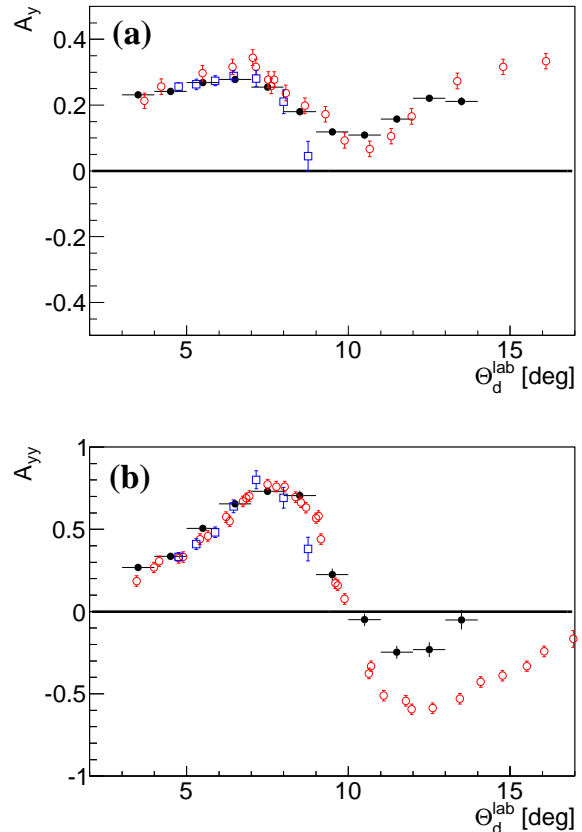


FIG. 1: (Color online) Angular distributions of vector (A_y , top) and tensor (A_{yy} , bottom) analyzing powers in dp scattering at $T_d = 2.27$ GeV. The filled circles denote results from this work, whereas open symbols denote results previously obtained at Argonne National Lab at $T_d = 2.0$ GeV [15] (open circles) and COSY-ANKE at $T_d = 2.27$ GeV [17] (open squares). The shown error bars denote statistical uncertainties.

weakly dependent on the beam energy. This is supported by very recent data obtained at COSY-ANKE [17] at $T_d = 2.27$ GeV. As a result we obtain beam polarizations of $P_z = 0.67(2)$, $P_{zz} = 0.65(2)$ for "up" and $P_z = -0.45(2)$, $P_{zz} = 0.17(2)$ for "down".

Checks of Quasifree Scattering

The vector polarization of the beam for quasifree scattering has been checked by quasifree pp scattering, which also was measured in parallel by detecting one of the protons in the forward detector and the other one in the central detector – and, in addition, checking their angular correlation for elastic kinematics. If the proton in the beam deuteron is at rest, then its momentum corresponds to just half of the beam momentum. Note that in the energy region of interest here, the pp analyzing power does not exhibit any significant energy dependence, hence we

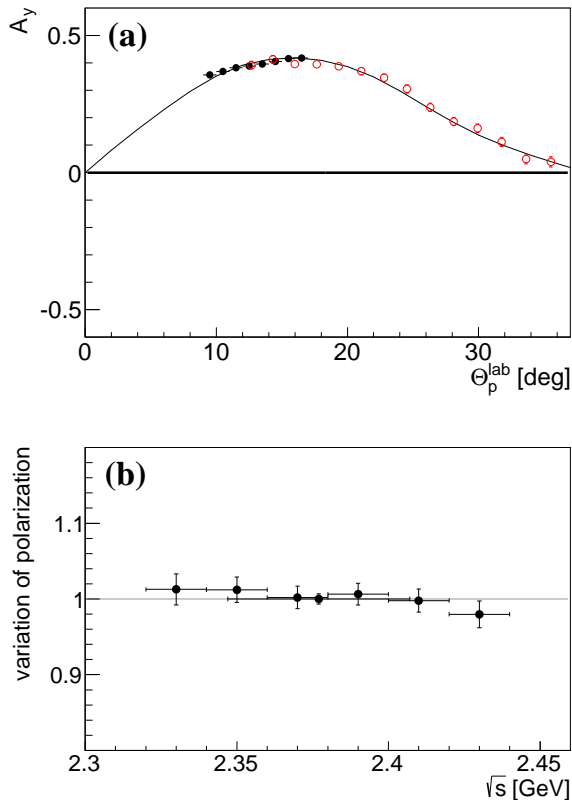


FIG. 2: (Color online) Top: Vector analyzing power A_y in pp scattering at $T_p = 1.135$ GeV. Filled circles denote results from this work, whereas open symbols denote results previously obtained with EDDA at $T_p = 1.1316$ GeV [18]. The solid line represents the SAID SP07 phaseshift solution [19]. Bottom: Variation of the proton polarization over the measured energy interval in relation to the SAID SP07 phase shift solution. The datum at 2.377 GeV derives from the figure shown at the top and denotes the average over the full energy range covered in this experiment.

do not need to correct for the energy smearing due to the Fermi motion of the proton. Fig. 2 shows our results from the quasifree pp scattering for the analyzing power. On top the angular distribution is shown in comparison with the EDDA measurements [18] of free pp scattering. The solid curve gives the SAID phase shift solution SP07 [19], which again is based in this energy range on the EDDA data.

In order to check, whether the proton polarization depends on the effective energy of the quasifree incident protons, we reconstruct the effective center-of-mass energy \sqrt{s} for each event. That way we obtain angular distributions sorted in six \sqrt{s} bins, which we compare to SAID SP07 phase shift predictions for these energies. The ratio of our pp data to the SAID prediction at each of these energies is plotted in Fig. 2, bottom. Within uncertainties no deviation from unity is observed, *i.e.*, the proton polarization can be considered to be constant

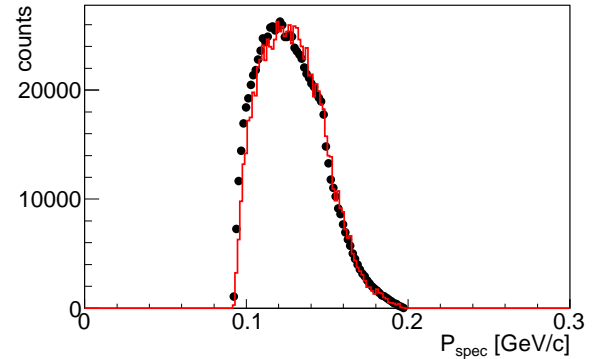


FIG. 3: (Color online) Distribution of the spectator proton momenta (in the deuteron rest frame) in the $dp \rightarrow pn + p_{\text{spectator}}$ reaction within the acceptance of the WASA detector. Data are given by the full circles. The solid line shows the expected distribution for the quasifree process based on the CD Bonn potential [20] deuteron wavefunction. For the data analysis only events with $p_{\text{spectator}} < 0.16$ GeV/c have been used.

within 1 % over the energy interval covered by this experiment.

The momentum distribution of the observed spectator proton in the elastic np scattering process is plotted in Fig. 3 in the deuteron rest frame, where it is compared with Monte Carlo simulations of the proton momentum distribution in the deuteron filtered by the acceptance of the WASA detector. In these simulations the CD Bonn potential [20] deuteron wavefunction has been used. Due to the beam-pipe ejectiles can only be detected in the forward detector for lab angles larger than three degrees. In order to assure a quasi-free process we omit events with spectator momenta larger than 0.16 GeV/c (in the deuteron rest system) from the subsequent analysis – as done in previous work [2–4].

RESULTS AND DISCUSSION

A_y Angular Distributions

Since we have measurements with spin "up", "down" and unpolarized, the vector analyzing power for np scattering can be derived in three different ways by using each two of the three spin situations. All three methods should give the same results. Differences in the results may be taken as a measure of systematic uncertainties, which are added quadratically to the statistical ones to give the total uncertainties.

In Fig. 4 we show the results for A_y , if we either combine measurements with spin "up" and unpolarized (open circles) or with spin "down" and unpolarized (solid squares) for extracting A_y . The values for the combina-

tion "up" and "down" are just in between (solid circles). For this plot the data are used without accounting for the spectator momentum, *i.e.* without selection according to the np center-of-mass energy. Thus this data set corresponds to the weighted average over the covered interval of \sqrt{s} .

Due to the Fermi motion of the nucleons bound in the beam deuteron, the measurement of the quasi-free np scattering process covers a range of energies in the np system. Meaningful statistics could be collected for the range of np center-of-mass energies $2.37 < \sqrt{s} < 2.40$ GeV corresponding to $T_n = 1.11 - 1.20$ GeV.

By taking into account the measured spectator four-momentum we may construct the effective \sqrt{s} for each event. That way we obtain angular distributions sorted in \sqrt{s} bins. In order to have sufficient count-rate statistics we restricted this procedure to the data sets in the angular region $31^\circ < \Theta_n^{cm} < 129^\circ$ and divided the available energy range into six bins, which are shown in Fig. 5 together with the SAID SP07 solution (solid lines) and the new solution – see next section – which contains a resonance pole (dashed and dotted lines). We also include in Fig. 5 previously obtained angular distributions at $\sqrt{s} = 2.360$ and 2.440 GeV ($T_n = 1.095$ and 1.27 GeV) [8–11], which are closest to the resonance region covered here. Note, that these angular distributions being below and above the resonance region exhibit a significantly different angular behavior – in particular at medium angles.

In Fig. 6 we show as an example the energy dependence of A_y at $\Theta_n^{cm} = 70^\circ$ — see also Fig. 4 in Ref. [12], where the energy dependence at $\Theta_n^{cm} = 83^\circ$ is depicted. The trend of the new data in the resonance region deviates clearly from that exhibited by the data from previous experiments below and above this region [8–10, 22–27]. The new partial-wave solutions (see below) connect all data within their uncertainties, whereas the SP07 solution obviously fails in the resonance region.

The decomposition of the np -scattering observables into partial wave amplitudes is given in Ref. [21]. Accordingly we have for the analyzing power:

$$d\sigma/d\Omega * A_y \sim \text{Im}(H_3 + H_5)H_4^* \quad (2)$$

with H_i containing sums over partial wave amplitudes with total angular momenta $j_0 = j = L$, $j_- = L - 1$ and $j_+ = L + 1$. H_3 contains terms being proportional either to the Legendre polynomials P_j or to the associated ones P_j^1 . In H_5 there are terms only proportional to P_j and in H_4 only proportional to P_j^1 . In particular, the structure of H_4 for $j = 3$ is as follows:

$$H_4(j = 3) \sim [4(T_{L=4} - 3T_{L=2}) + \sqrt{12}T_{L=3}]P_3^1, \quad (3)$$

where the T-matrix elements contain the complex phase shifts. We see that a resonance effect in 3D_3 and 3G_3 enters with opposite sign and is proportional to P_3^1 in both

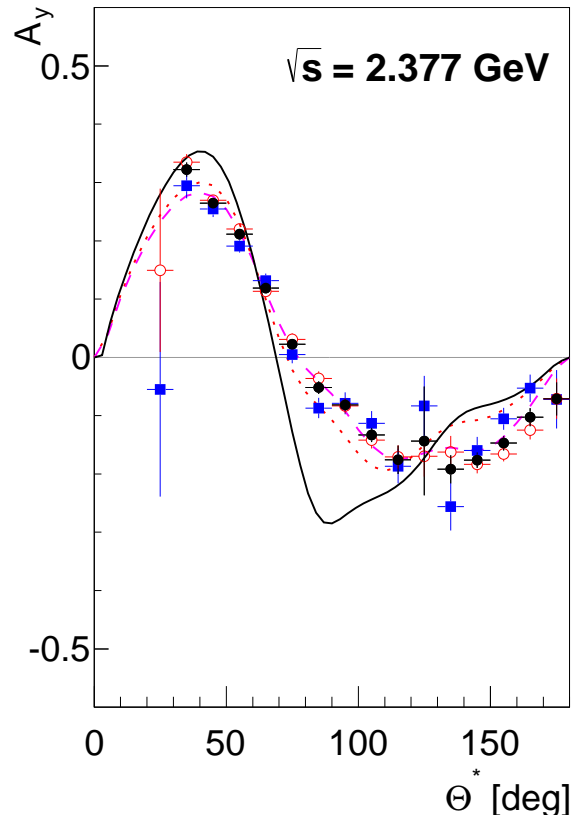


FIG. 4: (Color online) Angular distributions of the np analyzing power without consideration of the spectator momentum, *i.e.* without classifying the collected pn scattering events according to their effective total center-of-mass energy \sqrt{s} . That way the data set corresponds to the weighted average over the measured interval representing effectively the range $\sqrt{s} = 2.377 \pm 0.03$ GeV (corresponding to $1.075 \text{ GeV} \leq T_n \leq 1.195$ GeV). Open circles and solid squares denote the A_y extraction by the combination "up" with "unpolarized" and "down" with "unpolarized", respectively. The solid circles give the statistically weighted average over both methods. The error bars denote statistical uncertainties. The solid line represents the SAID SP07 phase shift solution [19], whereas the dashed (dotted) line gives the result of the new weighted (unweighted) SAID partial-wave solution, see text.

cases. Hence the resonance effect vanishes at the zeros of P_3^1 , which is the case at $\Theta = 63.4^\circ$ and 116.6° . At these angles the predictions with and without resonance in 3D_3 or 3G_3 should cross each other. If in the SP07 solution and in the new solution the non-resonant contributions are comparable, then the angular distributions calculated with these solutions should cross at these angles. Fig. 5 demonstrates that this is the case in good approximation.

By observing the maximum deviations from the SP07

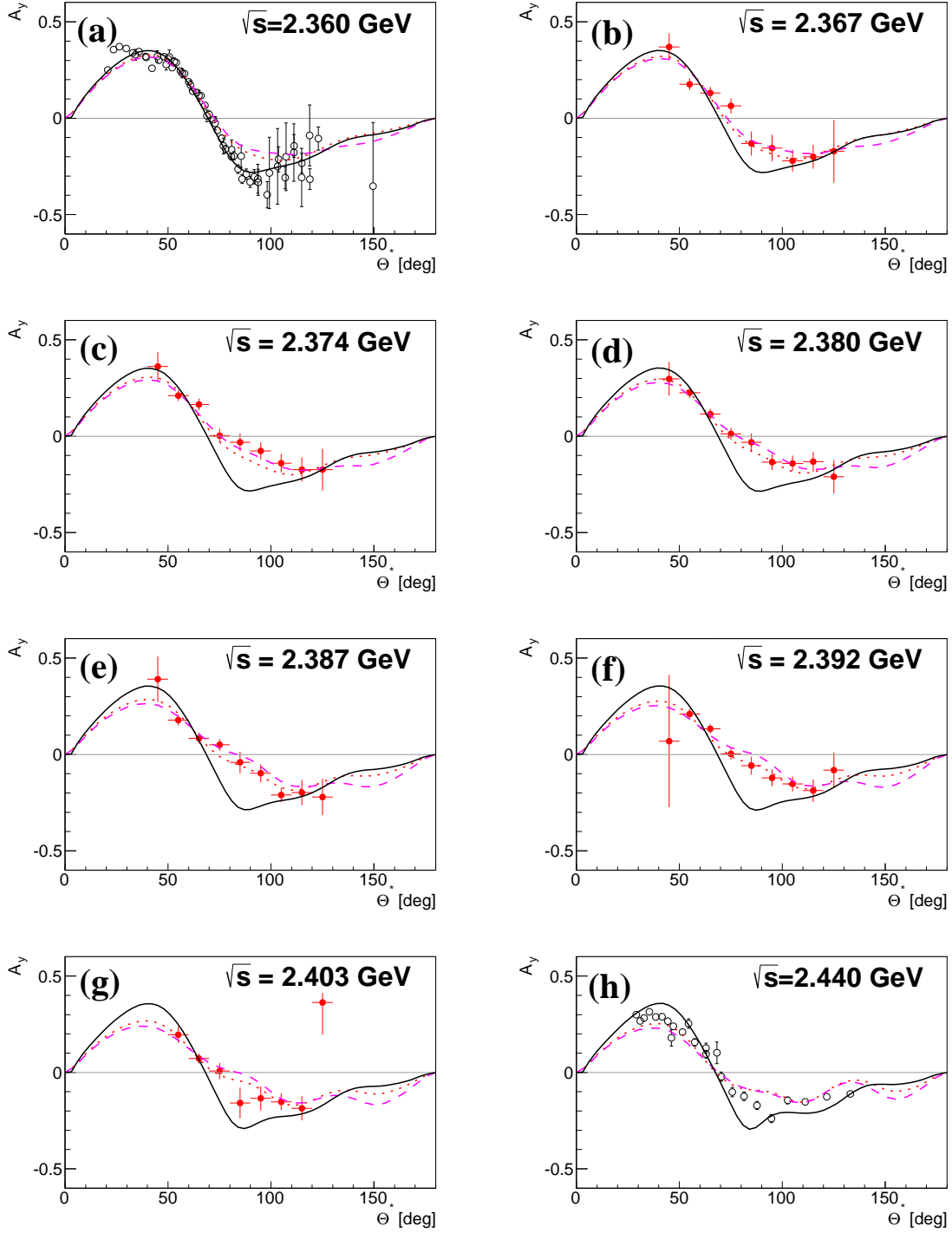


FIG. 5: (Color online) A_y angular distributions for $\sqrt{s} = 2.360, 2.367, 2.374, 2.380, 2.387, 2.392, 2.403$ and 2.440 GeV corresponding to $T_n = 1.095, 1.108, 1.125, 1.139, 1.156, 1.171, 1.197$ and 1.27 GeV. The full symbols denote results from this work taking into account the spectator four-momentum information. The error-bars on the full symbols include both statistical and systematic uncertainties. The open symbols denote previous work [8–11]. The solid lines represent the SAID SP07 phase shift solution [19], whereas the dashed (dotted) lines give the result of the new weighted (unweighted) SAID partial-wave solution, see text.

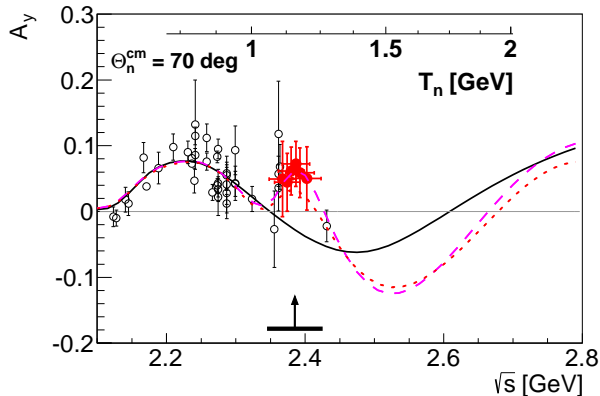


FIG. 6: (Color online) Energy dependence of the np analyzing power at $\Theta_n^{cm} = 70^\circ$. The solid symbols denote the results of this work, the open symbols denote those from previous work [8–10, 22–27]. For the meaning of the curves see Fig. 4. Vertical arrow and horizontal bar indicate pole and width of the resonance.

solution in the angular region around 90° as well as the minimum deviations around 63° and 117° – coupled with a sign change thereafter – both data and new SAID solutions exhibit the characteristic features of the P_3^1 function and thus uniquely point to the signature of a $J^P = 3^+$ resonance in the elastic np scattering.

The horizontal bars on the data points in Fig. 6 (and also in Fig. 4 of Ref. [12]) include both the range of the \sqrt{s} bins and the uncertainties in the determination of the \sqrt{s} values reconstructed for each event. Since we deal here only with 0 - 2 overconstraints in the kinematic fits, the \sqrt{s} determination is less precise than, *e.g.*, in the $pd \rightarrow d\pi^0\pi^0 + p_{spectator}$ reaction, where we have three overconstraints in the case that the proton spectator is not detected.

Partial-Wave Analysis

The new A_y data have been included in the SAID database and the phenomenological approach used in generating the NN partial-wave solution, SP07 [19], has been retained. Here we are simply considering whether the existing form is capable of describing the new A_y measurements. One advantage of this approach is that the employed Chew-Mandelstam K-matrix can produce a pole in the complex energy plane without the explicit inclusion of a K-matrix pole in the fit form. Neither the existence of a pole nor the effected partial waves are pre-determined.

The energy-dependent fits use a product S-matrix approach as described in detail in Ref. [28] with S_x being an ‘exchange’ part, including the one-pion-exchange piece, plus smooth phenomenological terms, and S_p , a

‘production’ part. The full S matrix is

$$S = S_x^{1/2} S_p S_x^{1/2} = 1 + 2iT, \quad (4)$$

where

$$T = T_x + S_x^{1/2} T_p S_x^{1/2}. \quad (5)$$

For spin-uncoupled waves, the production T-matrix is parameterized using a Chew-Mandelstam K-matrix, as is also used in the GW πN [29] and KN [30] analyses, with

$$T_p = \rho^{1/2} K_p (1 - CK_p)^{-1} \rho^{1/2}, \quad (6)$$

where ρ is a phase space factor, K_p is a real symmetric matrix coupling the NN and an inelastic channel, and C is a Chew-Mandelstam matrix. For isovector waves, the inelastic channel is identified as $N\Delta$; in the isoscalar case, this inelastic channel is generic. For spin-uncoupled waves, the matrices are 2×2 ; for coupled waves, the matrices are 3×3 , as described in Ref. [28]. The global energy-dependent fit includes pp data from threshold up to a lab kinetic energy of 3 GeV, and np data from threshold up to 2 GeV. Since above 1.3 GeV the amount of np data is sparse, the fit is considered to be valid only up to 1.3 GeV for the np case. Single-energy (narrow energy bin) fits are also carried out, with constraints on the energy-dependence over a particular energy bin fixed to the underlying global analysis.

The new A_y data are angular distributions at T_{Lab} values of 1.108, 1.125, 1.135, 1.139, 1.156, 1.171, and 1.197 GeV. Starting from the functional form of the current SP07 fit, and only varying the associated free parameters, a χ^2/datum of 1.8 was found for all angular distributions apart from the one at 1.135 GeV. This is fairly consistent with the overall χ^2/datum given by the global fit of np to 2 GeV. However, the set at 1.135 GeV contributes a χ^2/datum of about 25, has better statistics and a wider angular coverage.

The fit form was scanned to find partial waves for which an added term in the K-matrix expansion produced the most efficient reduction in χ^2 . Adding parameters and re-fitting resulted in a rapid variation of the coupled 3D_3 and 3G_3 waves in the vicinity of the problematic 1.135 GeV data set.

Some weighting seemed necessary in this fit, as only a few angular points from the full set were determining the altered energy dependence. The fit was repeated with different weightings (with a factor of 2 or 4) for the new A_y data. Initially, the full set of energies was weighted equally. However, it was found that just weighting the 1.135 GeV angular distribution improved the fit to the new analyzing power data at all energies. The results reported here thus considered only the weighting at this single energy. As we have seen in fits to other reactions, heavily weighting new and precise polarization observables inevitably degrades the fit to older data. Therefore,

as a test, the parameterization producing a pole was refitted to the full database with no weighting. This gave, as expected, a worse fit to the 1.135 GeV angular distribution but did not change the shape qualitatively.

In Figs. 4 - 6 and 9 - 11 we plot the SP07 prediction (not including the new data), a weighted fit (errors decreased by a factor of 4), and an unweighted fit including the new data and using the fit form having added parameters.

Resulting changes in the 3D_3 - 3G_3 coupled waves have been displayed already in Ref. [12], Fig. 3. Note that the single-energy solutions obtained previously for energies up to 1.1 GeV fit better to the new partial-wave solution than to SP07.

In the new solution the 3D_3 wave obtained a typical resonance shape, whereas the 3G_3 wave changed less dramatically. In Fig. 7 the Argand diagrams of the new partial-wave solution are shown for 3D_3 and 3G_3 partial waves as well as for their mixing amplitude ϵ_3 . In the Argand diagram the 3D_3 partial wave exhibits an abrupt change at the pion production threshold ($\sqrt{s} = 2.02$ GeV), when absorption sets in, followed by a pronounced looping in the d^* energy region, before it enters the region of the conventional t -channel $\Delta\Delta$ process [1-4] at the highest energies. In the Argand diagrams of 3G_3 and ϵ_3 also a looping is observed in the d^* region, though much less pronounced.

A search of the complex energy plane revealed a pole in the coupled 3D_3 - 3G_3 wave. Other partial waves did not change significantly over the energy range spanned by the new data.

The fit repeated with different weightings for the new A_y data resulted in a variation of the pole position and could be considered a minimal 'error' on its value within the present fit form. In the weighted fits, a pole was located at $(2392 - i37)$ MeV. The re-fit without weighting produced a pole with $(2385 - i39)$ MeV.

For the 3D_3 partial wave we display in Fig. 8 a speed plot as defined in Refs. [31, 32]. It exhibits a Lorentz-like shape with a maximum at 2.37 GeV and a width of about 80 MeV. Hence together with the speed-plot determination we arrive at $(2380 \pm 10 - i40 \pm 5)$ MeV as our best estimate for the pole position.

As pointed out by Höhler [31] both Argand diagram and speed plot allow also the determination of the modulus r of the residue, which corresponds to just half of the partial decay width Γ_{el} of the resonance into the elastic channel. Since according to Höhler the radius of the resonance circle in the Argand diagram equals to just half the branching ratio $B_{el} = \Gamma_{el}/\Gamma$, we derive from the Argand diagram plotted in Fig. 7, top, a value of $B_{el} = 0.15$. The height H of the Lorentz-like peak above background in the speed plot is related to the branching ratio by $H = 2B_{el}/\Gamma$, which leads to $B_{el} = 0.10$. These numbers depend, of course, somewhat on the assumption of the background. Hence, as our best estimate for the branching ratio we take the average $B_{el} = 0.12 \pm 0.03$

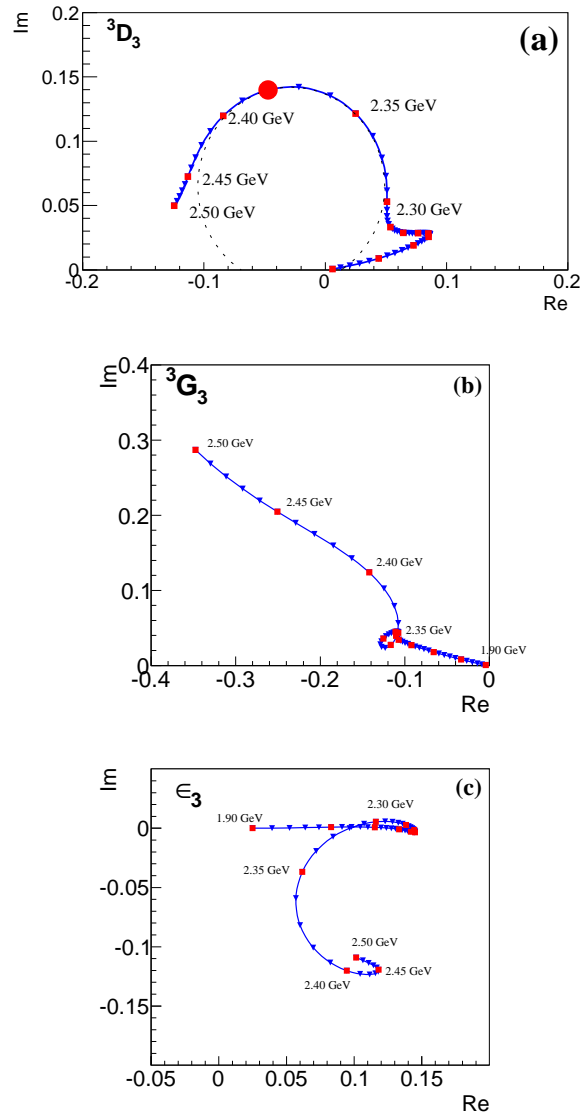


FIG. 7: (Color online) Argand diagrams of 3D_3 (top) and 3G_3 (middle) partial waves as well as of their coupling amplitude ϵ_3 (bottom) in the new partial-wave solution. Values are plotted as small solid triangles in 10 MeV steps and as small squares in 50 MeV steps together with the corresponding total energy \sqrt{s} . The thick solid circle gives the energy position of the resonance pole. The dotted curve in the top figure is a circle fitted to the loop, its diameter equals to the branching ratio B_{el} .

(corresponding to $r = 5 \pm 1$ MeV). This value agrees very well to the expectation based on unitarity and the knowledge about the various two-pion decay channels of the intermediate $\Delta\Delta$ system, which d^* decays into [7].

In addition to the modulus r of the residue also its phase Φ can be determined - most favorably from the Argand diagram of the derivative of the partial-wave amplitude [31, 32] - though usually with much lower accuracy. Here, we obtain values for Φ between -21 and $+9$ degrees,

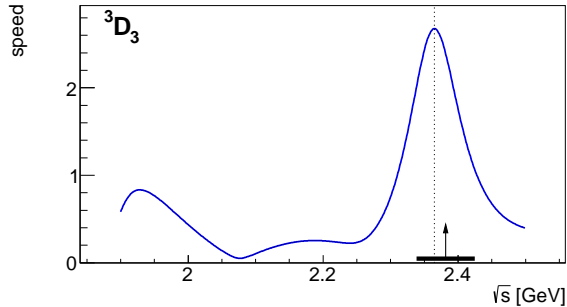


FIG. 8: (Color online) Speed plot of the 3D_3 partial wave. The dotted vertical line indicates the position of the maximum. Vertical arrow and horizontal bar indicate pole and width of the resonance as average over the values obtained in contour and speed plots, see text.

depending on details of the procedure.

COMPARISON OF THE NEW PARTIAL-WAVE SOLUTION TO FURTHER OBSERVABLES OF NEUTRON-PROTON SCATTERING

In the following we compare the new SAID partial-wave solution to all data related to the np scattering issue, which are available for the energy region of interest.

Total Cross Section

In Ref. [7] the contribution of the d^* resonance to the total np cross section has been estimated to be around 1.5 mb. Though this is small compared to the total cross section of 38 mb in the resonance region, it is larger than the uncertainties quoted in the total cross section measurements of Devlin *et al.* [34]. In fact, the total np cross section data exhibit a significant rise in this region, whereas the total pp cross section is flat in the region of interest.

Fig. 9, top, shows the total np cross section for $T_n = 0.5 - 1.5$ GeV. The data plotted by open squares for $T_n < 0.8$ GeV are from Lisowski *et al.* [33] taken at LAMPF in a high-resolution dibaryon search. The other data plotted by open triangles are from Devlin *et al.* [34] taken with a neutron energy resolution of (4 - 20)% (horizontal bars in Fig. 5). Also data from Sharov *et al.* [35] are shown (open circles), which have larger uncertainties, but are taken with a much superior neutron energy resolution of (13 - 15) MeV. The data exhibit a pronounced jump in the cross section between $T_n = (1.0 - 1.3)$ GeV. This jump is remarkable, since the pp total cross section is completely flat in this energy region. Hence in the isoscalar total nucleon-nucleon cross section $\sigma_{I=0} = 2\sigma_{pn} - \sigma_{pp}$, where the SAID values are

used for σ_{pp} , this effect appears still more pronounced (Fig. 9, bottom). The current SAID SP07 solution is shown by the solid lines again. Its description of the data is only fair. In particular the observed increase in the total cross section above 1 GeV is only slightly indicated in the SAID SP07 solution. The dotted lines show the new weighted partial-wave solution, which includes the resonance pole. They exhibit a clear s -shaped resonance behavior. The dashed lines are averaged over the experimental resolution of the data of Devlin *et al.* [34] and provide a preferable description of the data.

In Fig. 10 we show total np cross sections measured in dependence of the spin directions of beam and target particles. These spin-dependent total cross sections are measured with the directions of beam and target polarizations being either parallel or antiparallel. For the so-called transversal total cross section difference $\Delta\sigma_T$ the polarization vectors are transversally oriented with respect to the beam direction. For the so-called longitudinal cross section difference $\Delta\sigma_L$ they are longitudinally oriented.

For $\Delta\sigma_T$ there exist measurements for energies below the resonance region only, but for $\Delta\sigma_L$ measurements extend to energies well above this region. Whereas SP07 and new solutions nearly coincide below and in the resonance region for $\Delta\sigma_T$, they deviate substantially from each other for $\Delta\sigma_L$. On average the new solution gives a superior description of the $\Delta\sigma_L$ data, in particular in and above the resonance region.

Differential Cross Section

Fig. 11 shows the angular distribution of the differential cross section $d\sigma/d\Omega$ for elastic np scattering at $T_n = 1.135$ GeV corresponding to the resonance energy $\sqrt{s} = 2.38$ GeV, where we expect the effect of the resonance on the observables to be largest. At this energy there are only data for the differential cross section at very forward and backward scattering angles. The solid line denotes the current SAID SP07 solution, the dashed (dotted) line gives the result with the new weighted (unweighted) SAID solution. The resonance effect is small though noticeable in the differential cross section, since in contrast to the analyzing power the partial-wave amplitudes enter only quadratically. The resonance effect is predicted to be most notable at intermediate angles, where the differential cross section gets smallest and where as of yet no data are available.

Spin-Correlation and Spin-Transfer Observables

As of yet there are no direct measurements of spin-correlation and spin-transfer measurements in the resonance region. However, at COSY-ANKE the reaction

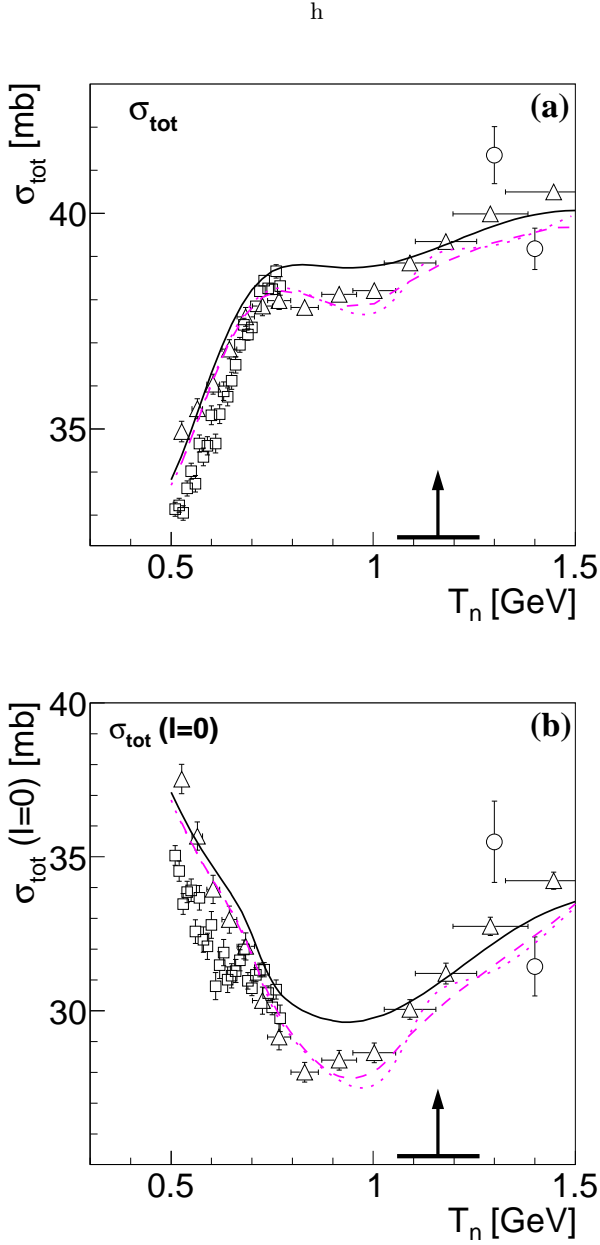


FIG. 9: (Color online) Total pn cross section (top) and total isoscalar nucleon-nucleon cross section (bottom) in dependence of the incident neutron (nucleon) energy T_n . Data are from Lisowski et al. [33] (open squares), Devlin et al. [34] (open triangles) and Sharov et al. [35] (open circles). The horizontal bars indicate the energy resolution of the incident neutrons. Solid and dashed curves representing the SP07 and the new solution, respectively, are averaged over the experimental energy resolution of Ref. [34]. The dotted line gives the new solution without averaging over the experimental energy resolution. Vertical arrow and horizontal bar indicate pole and width of the resonance.

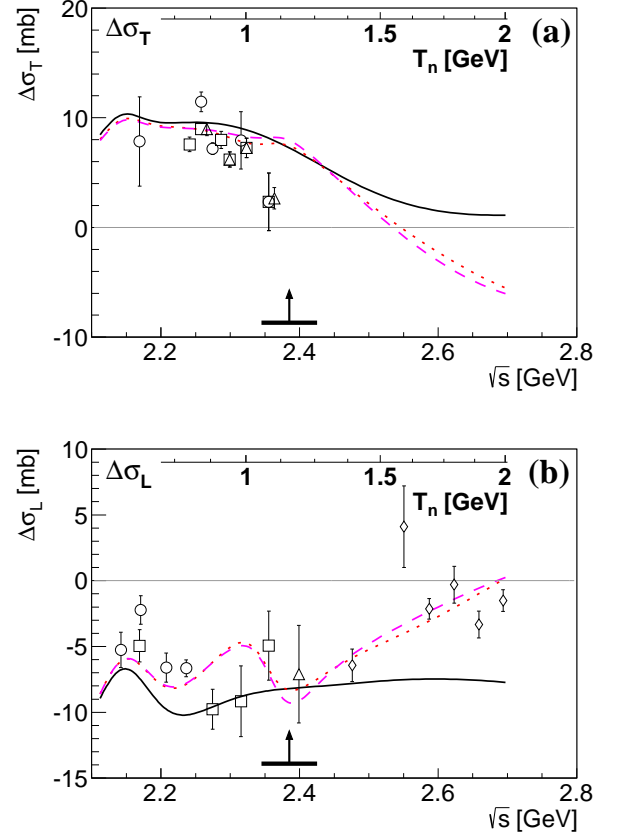


FIG. 10: (Color online) Energy dependence of the transversal (top) and longitudinal (bottom) total np cross section differences. The symbols denote data from Refs. [9, 35–40]. For the meaning of the curves see Fig. 4. Vertical arrow and horizontal bar indicate pole and width of the resonance.

$d\vec{p} \rightarrow n[pp]_s$ has been measured at various energies [43], where $[pp]_s$ means the proton pair to be in relative 1S_0 state. At ANKE this has been achieved experimentally by requiring the relative kinetic energy of the two protons to be smaller than 3 MeV.

This reaction is correlated with np scattering in the impulse approximation. Whereas the obtained polarization observables agree very well to calculations based on the SAID SP07 solution for $T_d < 2$ GeV, these measurements show large deviations at $T_d = 2.27$, which corresponds just to the resonance energy. A simple relation of the ANKE polarization observables to specific ones of np scattering is obtained in the pp 1S_0 limit at $\Theta_n^{cm} = 180^\circ$ [44] for the deuteron-proton tensor analyzing powers

$$\begin{aligned}
 A_{xx}(q=0) &= A_{yy}(q=0) = \\
 &= 2 \frac{K_{0l0}(\pi) - K_{0nn0}(\pi)}{3 - K_{0l0}(\pi) - 2K_{0nn0}(\pi)}
 \end{aligned} \tag{7}$$

and spin-correlation parameters

SUMMARY AND CONCLUSIONS

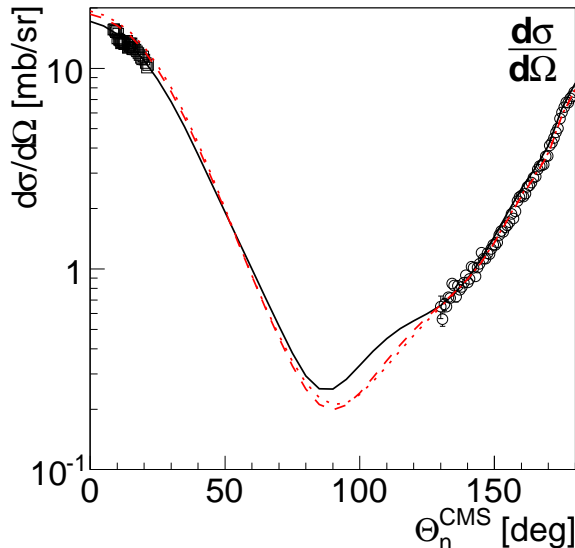


FIG. 11: (Color online) Angular distribution of the differential cross section $d\sigma/d\Omega$ at $T_n = 1.135$ GeV corresponding to the resonance energy $\sqrt{s} = 2.38$ GeV. For the meaning of the curves see caption of Fig. 4. The plotted data are from Ref. [41] ($T_n = 1.135$ GeV) and Ref. [42] ($T_n = 1.118$ GeV).

TABLE I: Deuteron-proton tensor analyzing powers and spin-correlation parameters at $T_d = 2.27$ GeV and $q = 0$ obtained from SAID SP07 [19] and new partial-wave solutions by use of eqs. (4) - (5) in comparison with experimental results from COSY-ANKE [43].

observable	experiment	SP07	new solution
$A_{xx}(0) = A_{yy}(0)$	-0.38(3)	-0.30	-0.42
$C_{x,x}(0) = C_{y,y}(0)$	-0.39(5)	-0.48	-0.31

$$\begin{aligned}
 C_{x,x}(q=0) &= C_{y,y}(q=0) \\
 &= 2 \frac{A_{00nn}(\pi) - D_{n0n0}(\pi)}{3 - K_{0l10}(\pi) - 2K_{0nn0}(\pi)},
 \end{aligned}
 \tag{8}$$

where q is the momentum transfer between initial neutron and final proton. Here A_{ijkl} , D_{ijkl} and K_{ijkl} denote neutron-proton spin correlation and spin-transfer parameters.

ANKE finds $A_{xx} = -0.38(3)$ and $C_{x,x} = -0.39(5)$ at $T_d = 2.27$ GeV (Table 1). Calculating these observables with the SP07 solution results in values -0.30 and -0.48, respectively, which are significantly different. However, the new SAID solution gives $A_{xx} = -0.42$ and $C_{x,x} = -0.31$, which are closer to the ANKE experimental values.

The exclusive and kinematically complete measurements of quasifree polarized neutron-proton scattering with WASA at COSY have provided detailed high-statistics data for the analyzing power in the energy range, where a narrow resonance structure with $I(J^P) = 0(3^+)$, called d^* , was observed previously in the double-pionic fusion to the deuteron. A partial-wave analysis including these new data exhibits a resonance pole at $(2380 \pm 10 - i40 \pm 5)$ MeV in the 3D_3 - 3G_3 coupled partial waves – establishing thus the $d^*(2380)$ resonance structure to be a genuine s -channel resonance. This constitutes the first clear-cut experimental finding of a true dibaryon resonance.

This resonance has been first observed in the reaction $pn \rightarrow d\pi^0\pi^0$ reaction. The Dalitz plot there [2] shows that the resonance predominantly decays via an intermediate $\Delta\Delta$ configuration. Exactly such a state with identical quantum numbers has been predicted first by Dyson and Xuang [45] based on SU(6) symmetry breaking already in 1964 – just shortly after Gell-Mann's publication of the quark model [46]. Whereas this dibaryon state was denoted by D_{03} in Ref. [45], it was named d^* later-on by Goldman *et.al.* [5], who pointed out the unique symmetry properties of such a state with these quantum numbers calling it the "inevitable" dibaryon.

So $d^*(2380)$ may be associated with a bound $\Delta\Delta$ resonance, which could contain a mixture of asymptotic $\Delta\Delta$ and six-quark, hidden color configurations [47]. Recent quark-model calculations [48–50] find this state at a mass close to the experimental one. Whereas the width calculated in Ref. [48] is still substantially too large, the one obtained in Ref. [50] is already in good agreement with the experimental finding, as soon as coupling to hidden color configurations is accounted for. New three-body calculations [51, 52] of Faddeev type with relativistic kinematics and hadron dynamics find $d^*(2380)$ at the right mass and only slightly larger width [58].

In addition to np scattering evidence for d^* has been found so far in the two-pion production reactions $pn \rightarrow d\pi^0\pi^0$, $pn \rightarrow d\pi^+\pi^-$ and $pn \rightarrow pp\pi^0\pi^-$. So the only remaining hadronic channels, where d^* should contribute, are $np\pi^0\pi^0$ and $np\pi^+\pi^-$. The first one has been studied at WASA and is on the way of being published. The latter channel has been measured at HADES and preliminary results have been reported already at conferences. This means that all major channels of the d^* decay will have been investigated in near future. All decay branches into the two-pion decay channels appear to be well accounted for by isospin relations [7].

It is amazing that the simple but basic estimate of Dyson and Xuong [45] is already very close to the now observed mass of d^* alias D_{03} . Together with the results of the new calculations based on quark [48–50] and/or

hadron dynamics [51, 52] this might give some confidence in the predictive power of these theoretical considerations on further dibaryon states.

We finally note that very recently an alternative explanation of the WASA data has been suggested by D. V. Bugg [53]. Among the issues raised in this paper we just mention here one. The specific intermediate $NN^*(1440)$ system proposed for the production of the narrow resonance-like structure is not restricted to the isoscalar channel and hence should show up both in np and pp initiated two-pion production. However, as we have shown, this narrow resonance structure is missing in all pp -initiated two-pion production channels including double-pionic fusion [3, 54–57].

ACKNOWLEDGMENTS

We acknowledge valuable discussions with J. Haidenbauer, Ch. Hanhart, A. Kacharava and C. Wilkin on this issue. This work has been supported by BMBF, Forschungszentrum Jülich (COSY-FFE), the U.S. Department of Energy Grant DE-FG02-99ER41110, the Polish National Science Centre (grant No. 2011/03/B/ST2/01847) and the Foundation for Polish Science (MPD).

* present address: Albert Einstein Center for Fundamental Physics, University of Bern, Sidlerstrasse 5, 3012 Bern, Switzerland

† present address: Department of Physics and Astrophysics, University of Delhi, Delhi–110007, India

‡ present address: Institut für Kernphysik, Johannes Gutenberg–Universität Mainz, Johann–Joachim–Becher Weg 45, 55128 Mainz, Germany

§ present address: Department of Physics and Astronomy, University of Sheffield, Hounsfield Road, Sheffield, S3 7RH, United Kingdom

- [1] M. Bashkanov *et al.*, Phys. Rev. Lett. **102**, 052301 (2009).
- [2] P. Adlarson *et al.*, Phys. Rev. Lett. **106**, 242302 (2011).
- [3] P. Adlarson *et al.*, Phys. Lett. B **721**, 229 (2013).
- [4] P. Adlarson *et al.*, Phys. Rev. C **88**, 055208 (2013).
- [5] T. Goldman, K. Malman, G. J. Stephenson, K. E. Schmidt, and F. Wang, Phys. Rev. C **39**, 1889 (1989).
- [6] P. J. Mulders, Phys. Rev. D **26**, 3039 (1982).
- [7] A. Pricking, M. Bashkanov, H. Clement, arXiv:1310.5532 [nucl-ex].
- [8] J. Ball *et al.*, Nucl. Phys. A **559**, 489 (1993).
- [9] A. de Lesquen *et al.*, Eur. Phys. J. C **11**, 69 (1999).
- [10] Y. Makdisi *et al.*, Phys. Rev. Lett. **45**, 1529 (1980).
- [11] R. Diebold *et al.*, Phys. Rev. Lett. **35**, 632 (1975).
- [12] P. Adlarson *et al.*, Phys. Rev. Lett. **112**, 202301 (2014).
- [13] Chr. Bargholtz *et al.*, Nucl. Inst. Meth. A **594**, 339 (2008).
- [14] H. H. Adam *et al.*, arxiv: nucl-ex/0411038.
- [15] M. Haji-Saied *et al.*, Phys. Rev. C **36**, 2010 (1987).
- [16] J. Arvieux *et al.*, Nucl. Phys. A **431**, 613 (1984).
- [17] D. Mchedlishvili, Internal ANKE report (28), 2013; available from: http://collaborations.fz-juelich.de/ikp/anke/internal_notes/DM_rtdp.pdf
- [18] M. Altmeier *et al.*, Eur. Phys. J. A **23**, 351 (2005).
- [19] SAID data base <http://gwdac.phys.gwu.edu/>; R. A. Arndt *et al.*, Phys. Rev. C **76**, 025209 (2007).
- [20] R. Machleidt, Phys. Rev. C **63** 024001 (2001).
- [21] R.A. Arndt *et al.*, Phys. Rev. D **28**, 97 (1983).
- [22] C. R. Newsom *et al.*, Phys. Rev. C **39**, 965 (1989).
- [23] J. Ball *et al.*, Nucl. Phys. A **559**, 477 (1993).
- [24] J. Arnold *et al.*, Eur. Phys. J. C **17**, 67 (2000).
- [25] M. W. McNaughton *et al.*, Phys. Rev. C **48**, 256 (1993); **53**, 1092 (1996).
- [26] G. Glass *et al.*, Phys. Rev. C **47**, 1369 (1983).
- [27] M. L. Barlett *et al.*, Phys. Rev. C **27**, 682 (1983); **40**, 2697 (1989).
- [28] R.A. Arndt, J.S. Hyslop, L.D. Roper, Phys. Rev. D **35**, 128 (1987).
- [29] R.A. Arndt *et al.*, Phys. Rev. C **74**, 045205 (2006); R.L. Workman *et al.*, Phys. Rev. C **86**, 035202 (2012).
- [30] J.S. Hyslop *et al.*, Phys. Rev. D **46**, 961 (1992).
- [31] G. Höhler, π N Newsletter **9**, 1 (1993), ISSN 0942-4148.
- [32] O. Hanstein, D. Drechsel, L. Tiator, Phys. Lett. B **385**, 45 (1996).
- [33] P. W. Lisowski *et al.*, Phys. Rev. Lett. **49**, 255 (1982).
- [34] T. J. Devlin *et al.*, Phys. Rev. D **8**, 136 (1973).
- [35] V. I. Sharov *et al.*, Eur. Phys. J. C **37**, 79 (2004); **13**, 255 (2000).
- [36] F. Lehar *et al.*, Phys. Lett. B **189**, 241 (1987).
- [37] J. M. Fontaine *et al.*, Nucl. Phys. B **358**, 297 (1991).
- [38] J. Ball *et al.*, Z. Phys. C **61**, 53 (1994).
- [39] M. Beddo *et al.*, Phys. Rev. D **50**, 104 (1993).
- [40] B. P. Adiashevich *et al.*, Z. Phys. C **71**, 65 (1996).
- [41] Y. Terrien *et al.*, Phys. Rev. Lett. **59**, 1534 (1987).
- [42] G. Bizard *et al.*, Nucl. Phys. B **85**, 14 (1975).
- [43] D. Mchedlishvili *et al.*, Eur. Phys. J. A **49**, 49 (2013) and priv. comm.
- [44] F. Lehar and C. Wilkin, Eur. Phys. J. A **37**, 143 (2008).
- [45] F. J. Dyson, N.-H. Xuong, Phys. Rev. Lett. **13**, 815 (1964).
- [46] M. Gell-Mann, Phys. Lett. B **8**, 214 (1964).
- [47] M. Bashkanov, S. Brodsky, H. Clement, Phys. Lett. B **727**, 438 (2013).
- [48] H. Huang, J. Ping, F. Wang, Phys. Rev. C **89**, 034001 (2014).
- [49] X. Q. Yuan, Z. Y. Zhang, Y. W. Yu, P. N. Shen, Phys. Rev. C **60**, 045203 (1999).
- [50] F. Huang, Z. Y. Zhang, P. N. Shen and W. L. Wang, arXiv:1408.0458 [nucl-th].
- [51] A. Gal, H. Garcilazo, Phys. Rev. Lett. **111**, 172301 (2013).
- [52] A. Gal, H. Garcilazo, Nucl. Phys. A **928**, 73 (2014).
- [53] D.V. Bugg, Eur. Phys. J. A **50**, 104 (2014).
- [54] F. Kren *et al.*, Phys. Lett. B **684**, 110 (2010) and B **702**, 312 (2011); arXiv:0910.0995v2 [nucl-ex]
- [55] T. Skorodko *et al.*, Phys. Lett. B **695**, 115 (2011).
- [56] T. Skorodko *et al.*, Eur. Phys. J. A **47**, 108 (2011).
- [57] T. Skorodko, *et al.*, Phys. Lett. B **679**, 30 (2009).
- [58] In Refs. [51, 52] a width suppression factor has been introduced, which is at variance with our observations for the $d^* \rightarrow pp\pi^0\pi^-$ decay [4]. Hence only the values for the width without this factor should be compared to the

experimental one.